Ce and Ca/Nb doped Pd-mesocellular foam catalysts for gas-phase conversion of acetone to methyl isobutyl ketone

Grzelak, Kalina; Thumbayil, Rouzana Pulikkal; Kegnæs, Søren; Trejda, Maciej; Riisager, Anders

Published in:
Microporous and Mesoporous Materials

Link to article, DOI:
10.1016/j.micromeso.2021.111169

Publication date:
2021

Document Version
Peer reviewed version

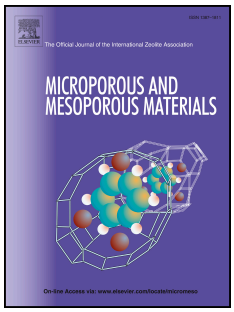

Ce and Ca/Nb doped Pd-mesocellular foam catalysts for gas-phase conversion of acetone to methyl isobutyl ketone

Kalina Grzelak, Rouzana Pulikkal Thumbayil, Søren Kegnæs, Maciej Trejda, Anders Riisager

PII: S1387-1811(21)00295-X

DOI: https://doi.org/10.1016/j.micromeso.2021.111169

Reference: MICMAT 111169

To appear in: *Microporous and Mesoporous Materials*

Received Date: 3 December 2020

Revised Date: 9 February 2021

Accepted Date: 10 May 2021

Please cite this article as: K. Grzelak, R.P. Thumbayil, Sø. Kegnæs, M. Trejda, A. Riisager, Ce and Ca/Nb doped Pd-mesocellular foam catalysts for gas-phase conversion of acetone to methyl isobutyl ketone, *Microporous and Mesoporous Materials* (2021), doi: https://doi.org/10.1016/j.micromeso.2021.111169.

Credit Author Statement

Kalina Grzelak: Investigation, Visualization, Writing - Original Draft.

Rouzana Pulikkal Thumbayil: Validation, Data Curation.

Søren Kegnæs: Resources.

Maciej Trejdaa: Conceptualization, Funding acquisition, Supervision.

Anders Riisager: Methodology, Project administration, Writing - Review & Editing.

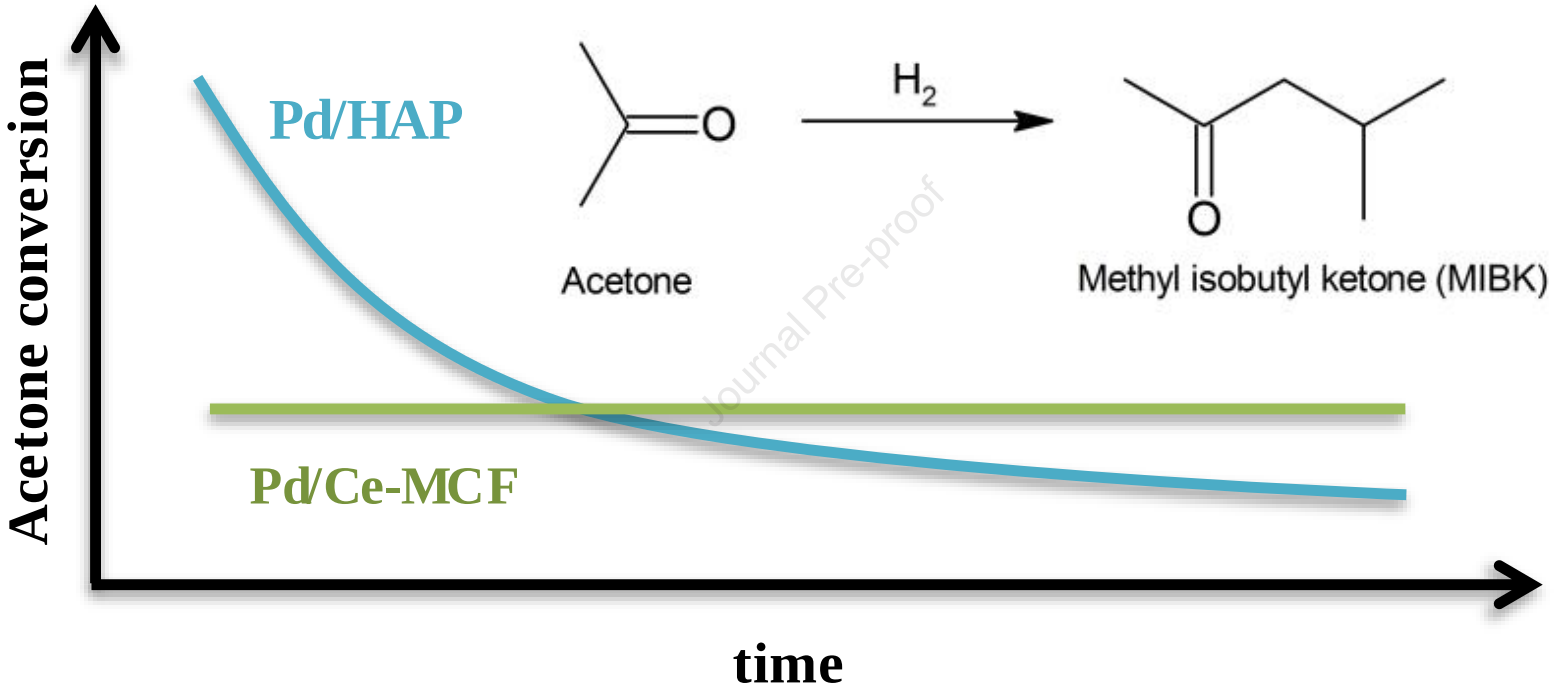

Ce and Ca/Nb doped Pd-mesocellular foam catalysts for gas-phase conversion of acetone to methyl isobutyl ketone

Kalina Grzelak,[a] Rouzana Pulikkal Thumbayil,[b] Søren Kegnæs,[b] Maciej Trejda[a,*] and Anders Riisager[b,*]

[a] Adam Mickiewicz University in Poznań, Heterogeneous Catalysis, ul. Uniwersytetu Poznańskiego 8, 61-614 Poznań, Poland.

[b] Centre for Catalysis and Sustainable Chemistry, Department of Chemistry, Technical University of Denmark, Kemitorvet, Building 207, 2800 Kgs. Lyngby, Denmark.

* Corresponding author contact: ar@kemi.dtu.dk, +45 4525 2233

* Corresponding author contact: tmaciej@amu.edu.pl, +48 61 8291807

Abstract

Herein, we report a study on the design of new palladium containing catalysts based on Ce- and Ca-Nb-mesocellular foam (MCF) supports for gas-phase conversion of acetone to methyl isobutyl ketone (MIBK). A comparison to other catalyst materials already described in the literature shows that the role of material structure (mesostructured cellular foams, hydroxyapatite or mesoporous aluminophosphate), acid-base character of the support, state of palladium species and the support metal dopants play important roles for the catalytic performance in the conversion of acetone to MIBK. Thus, the new catalytic system Pd/Ce-MCF with 11 % of conversion and 94 % of selectivity to MIBK

(250˚C) is demonstrated to be more attractive in term of stability for the reaction over time than previously described in literature for Pd/hydroxyapatite.

Keywords: Methyl isobutyl ketone; Acetone condensation; 2,5-hexanedione; Metal doped mesocellular foams; Palladium nanoparticles.

1. Introduction

Methyl isobutyl ketone (MIBK) is an industrially important chemical produced from acetone, which finds common use as a solvent for lacquers, resins or paints. The market size of MIBK was in 2018 estimated to USD 600 millions. In the industrial process for MIBK production, acetone undergoes self-condensation and dehydration and the obtained product is further hydrogenated to MIBK with hydrogen gas using palladium-doped cation exchange resins as the catalyst [1]. The application of a heterogeneous catalyst with bifunctional active sites can bridge the steps of this multi-step process, where the condensation reaction may be catalyzed by either acid or base. Various solid supports have been investigated for such an approach, including MgO [2], CaO [3], CeO_2 [4], Nb_2O_5/SiO_2 [5], zeolite HZSM-5 [6,7], Mg-Al mixed oxides [8], hydroxyapatite (HAP) [9], and its alkali metal ion exchanged derivatives [10], active carbon [11], oxynitride aluminophosphate (AlPON) [12], aluminophosphate (AlPO) and silicoaluminophosphate (SAPO) [13]. Among these, Rao et al. reported CeO_2 to be an effective basic support in acetone condensation which upon impregnation with nickel led to the formation of hydrogenation sites [4]. The Ni/CeO_2 catalyst with optimized nickel loading (2.5 wt%) gave 26 % of acetone conversion and 56 % of selectivity to

MIBK at 150 °C in a gas-phase reaction and the catalyst remained active for 10 h with only slight decrease in activity. Chen and coworkers investigated both acidic and basic supports for palladium nanoparticles, e.g. Nb_2O_5-SiO_2, SiO_2, Al_2O_3, CaO-Al_2O_3, SiO_2-Al_2O_3 and hydrotalcite in a liquid-phase reaction [5]. The best catalytic activity was obtained for Pd/Nb_2O_5-SiO_2 (0.1 wt% Pd and 27.4 wt% Nb_2O_5) with acetone conversion of 17 % and selectivity to MIBK of 92 % at 150 °C.

It is well-known that the support structure can play a crucial role for the dispersion of active sites and reactant diffusion in heterogeneous catalysts, and support materials with high surface area and defined morphology are therefore typically desired [14]. Mesoporous silicas belong to this group of materials and their porosity has previously been found to influence catalytic performance for several reactions due to enhanced mass transfer of 3D pore systems with interconnected cages, e.g. mesocellular foams (MCFs) and KIT-6, compared to 2D pore systems, e.g. SBA-15 [15–18]. However, such structure effect has not yet been explored for the one-step MIBK formation from acetone, and we decided therefore to exploit the use of MCF as a support material for palladium nanoparticles for conversion of acetone to MIBK. MCF materials have a unique structure consisting of quite large cells (20-40 nm) interconnected with windows that allow facile diffusion of substrate and products [19]. Previous work on doping silica MCF has shown that CeO_2 and CaO can be sources of basicity and Nb_2O_5 may act as a promoter to increase the basicity of active sites on CaO [20,21]. Here, we therefore studied the effect of introducing the elements Ce or Ca to MCF as main sources of basicity necessary for the condensation reaction. Moreover, the Ca-MCF catalyst was additionally doped with niobium which was proven to enhance catalytic performance when combined with calcium. Both catalysts were impregnated with palladium as an

active site for the final hydrogenation step in MIBK production. As a result, MCF doped with ceria or calcium and niobia were synthesized and applied as supports for palladium nanoparticles and the resulting Pd/Ce-MCF and Pd/Ca-Nb-MCF materials investigated as catalysts for the reductive condensation of acetone to produce MIBK (**Scheme 1**). Additionally, HAP and mesoporous aluminophosphate oxynitride (MAPN) modified with palladium served as reference catalysts, since those supports have been already reported in literature to be active for the MIBK formation [9,12]. In literature, Pd/HAP converted 17 % of acetone with 66 % of selectivity to MIBK at 150 °C [9], whereas Ni/MAPN yielded 80 % of selectivity to MIBK with 7 % of conversion at 200 °C [12].

2. Experimental

2.1 Syntheses

Mesocellular foam (MCF)

Pluronic P123 (16 g, Sigma Aldrich) was dissolved in 600 g of 0.7 M aqueous solution of hydrochloric acid at 33 °C, where after 1,3,5-trimethylbenzene (16 g, Sigma Aldrich) and ammonium fluoride (0.187 g, Sigma Aldrich) were added. After 1 h of stirring, tetraethyl orthosilicate (TEOS, 34.11 g, Sigma Aldrich) was added dropwise and the mixture stirred continuously at 33 °C for additional 20 h. Next, the mixture was placed in an oven at 100 °C for 24 h under static conditions, washed with water and then dried at 60 °C for 12 h. Finally, the template was removed by calcination at 500 °C for 8 h to obtain MCF. The MCF product was obtained with a yield of 97 %.

MCF doped with calcium and niobium (Ca-Nb-MCF) or cerium (Ce-MCF)

Calcium and niobium doped MCF was prepared by stepwise wetness impregnation of MCF using firstly an aqueous solution of niobium(V) oxalate (Sigma Aldrich, assumed 2 wt% of Nb loading) and secondly using an aqueous solution of calcium acetate monohydrate (Sigma Aldrich, assumed 20 wt% of Ca loading). The material was calcined at 500 °C for 5 h after impregnation with niobium and again at 700 °C for 5 h after impregnation with calcium.

Cerium doped MCF was done by impregnation of MCF with an aqueous solution of cerium(III) nitrate hexahydrate (Sigma Aldrich, assumed 20 wt% of Ce loading) followed by calcination at 500 °C for 5 h.

Hydroxyapatite (HAP), $Ca_5(PO_4)_3(OH)$

Hydroxyapatite was synthesized based on a literature procedure [22]. Calcium nitrate tetrahydrate (23.497 g, Sigma Aldrich) was dissolved in 166 mL of water, where after a solution of ammonium hydrogenphosphate (7.884 g in 149 mL of water) was added dropwise. The mixture was stirred at room temperature for 24 h keeping the pH at ~9.5 with addition of ammonia solution (25 % solution). Finally, the obtained white precipitate was filtered, dried and calcined at 600 °C for 5 h. The HAP product was obtained with a yield of 91 %.

Mesoporous aluminophosphate (MAP) and MAP oxynitride (MAPN)

MAP was prepared by dissolving Pluronic P123 (10 g, Sigma Aldrich) in 220 mL of ethanol followed by sequential addition of anhydrous aluminum chloride (6.670 g, Sigma Aldrich) and 3.4 mL of phosphoric acid (85 wt%) and continued stirring for 2.5

h. Afterwards, the mixture was slowly oven dried at 40 °C for 4 h and subsequently at 80 °C until complete evaporation of ethanol. Finally, the solid was calcined at 550 °C for 10 h. The MAP product was obtained with a yield of 99 %.

MAPN was prepared by treating the as-prepared MAP in a fixed-bed quartz reactor with pure ammonia gas flow at 800 °C for 24 h followed by cooling down in argon flow.

Palladium loaded catalysts

The prepared support materials were modified with palladium by incipient wetness impregnation for efficient loading of nominal palladium percentage [23,24]. The catalysts were impregnated with 3 wt% of palladium using aqueous solution of palladium(II) nitrate dihydrate (Sigma Aldrich) followed by drying and calcination at 550 °C for 4 h.

2.2 Characterization

Nitrogen adsorption/desorption isotherm were obtained using a Micromeritics ASAP 2020 apparatus at -196 °C after outgassing samples at 200 °C under vacuum. The surface area was determined by the BET method, pore parameters by the Broekhoff-de Boer method with BJH Fass correction (MCF), BJH method with Kruk-Jaroniec-Sayaroi correction (HAP) or DFT method with cylinder geometry (MAP, MAPN).

X-ray powder diffraction (XRD) was performed on a HuberG670 powder diffractometer using Cu Kα radiation within a 2Θ range of 20–80˚ in steps of 0.005˚.

X-ray photoelectron (XPS) spectra for Pd/Ca-Nb-MCF and Pd/Ce-MCF were collected on an ultra-high vacuum photoelectron spectrometer based on Phoibos 150 NAP analyzer (Specs, Germany). The analysis chamber was operated under vacuum with a pressure close to $5 \cdot 10^{-9}$ mbar and the sample was irradiated with a monochromatic Al Kα (1486.6 eV) radiation (15 kV; 10 mA). Binding energies were corrected by setting the Si 1s peak at 103.4 eV.

The XP spectra for Pd/HAP and Pd/MAPN were recorded on a Thermo Scientific K-Alpha system using Al Kα radiation (1484.6 eV) operating at the pressure of min. $8 \cdot 10^{-7}$ mbar. Binding energies were referenced to the C1s peak from the carbon surface deposit at 284.6 eV.

Temperature-programmed desorption of carbon dioxide (CO_2-TPD) was performed on Micromeritics Autochem II RS232 equipment. The sample (100 mg) was preheated at 550 °C (10 °C min^{-1}) in helium flow (25 cm^3 min^{-1}) for 1 h and the reactor cooled to 45 °C. Adsorption was then performed by passing CO_2 (15 cm^3 min^{-1}) diluted in helium (25 cm^3 min^{-1}) through the sample for 20 min followed by flushing with helium flow for 1 h. Thermal desorption of CO_2 was then recorded up to 550 °C with a thermal conductivity detector (TCD) every 1s using a heating ramp of 10 °C min^{-1}.

Transmission electron microscopy (TEM) images of powdered samples of Pd/Ce-MCF and Pd/HAP was recorded by a FEI Tecnai T20 microscope operating at 200 kV and on a Hitachi HT7700 microscope operating at 100 kV, respectively.

Scanning electron microscopy (SEM) image was carried out with a Quanta 250 FEG, FEI microscope operating at 10 kV.

2.3 Catalysis

Conversion of acetone to methyl isobutyl ketone (MIBK)

The catalytic conversion of acetone to MIBK was performed in gas-phase using a customized continuous-flow fixed-bed reactor setup described in detail elsewhere [7]. Pelletized catalyst (100 mg, grain size 180-355 μm) was positioned in a tubular quartz reactor (inner diameter 5 mm) and activated at 350 °C in a flow of hydrogen gas (50 cm^3 min^{-1}). Next the reactor was cooled to 150 °C and liquid acetone pumped (0.05 cm^3 min^{-1}), evaporated and mixed with pure hydrogen gas (50 cm^3 min^{-1}) into the reactor at ambient pressure. The reaction was carried out in the temperature interval 150-300 °C after keeping set temperatures for 1 h. Catalyst stability test was performed at 250 °C for 24 h. The gaseous reaction products were identified by GC-MS analysis and quantified by online GC-FID analysis (DB-1 column, 50 m × 0.32mm × 0.52μm).

Cyclisation and dehydration of 2,5-hexanedione (2,5-HDN)

The transformation of 2,5-hexanedione was conducted in a tubular fixed-bed down-flow reactor under atmospheric pressure using nitrogen as a carrier gas. The catalyst (50 mg) was activated at 350 °C for 2 h under nitrogen flow (50 cm^3 min^{-1}), and the reaction carried out at 350 °C by injecting 0.5 cm^3 of 2,5-HDN over 30 min into the catalyst by using a pump system (KD Scientific). The gaseous reaction products were analyzed by a SRI 310C chromatograph equipped with a capillary DB-1 column (30 m) and TCD detector.

3. Results and Discussion

3.1. Textural and structural properties

The successful synthesis of MCF was confirmed by SEM (Fig. S1) and nitrogen physisorption (Fig. S2), where mesoporous character of the support was evidenced by the isotherms of type IV(a) with hysteresis loop of IUPAC type H1 [25]. Modification of the MCF support with calcium and niobium (22 wt% in total) or cerium (20 wt%), led to a significant decrease in the surface area from 716 $m^2 g^{-1}$ for the parent material to 276 $m^2 g^{-1}$ for Ca-Nb-MCF and 487 $m^2 g^{-1}$ for Ce-MCF, respectively (Table 1). Although the pore volume, cell and window parameters decreased after the introduction of metals (Nb and Ca or Ce) implying at least partial pore blockage, the structure of the materials maintained mesoporous. Likewise, the pore volumes also slightly decreased after impregnation with palladium.

The hierarchical, hexagonal mesoporous structure of aluminophosphate (MAP) was confirmed by the isotherm of type IV(a) characteristic for materials with mesopores wider than 4 nm and hysteresis loop of type H1 indicating a narrow range of uniform pores. To increase the initial basicity, the MAP support was further modified by oxynitridation at high temperature (800 °C) by a flow of ammonia to obtain MAPN, which resulted in a decrease of surface area from 274 to 125 $m^2 g^{-1}$ (Table 1). According to literature, 800 °C is an optimal temperature to effectively incorporate nitrogen into the aluminophosphate structure [26–28]. For traditional AlPO this is not accompanied by a decrease in surface area [26,29,30], while this has been noted before for MAP [31]. This was also confirmed when the MAP support was heated to 800 °C and the surface area was reduced to 205 $m^2 g^{-1}$. Finally, the introduction of palladium (3 wt%) did not induce significant changes in the textural parameters of MAPN.

The structure of the second reference material, hydroxyapatite (HAP) was identified by XRD revealing typical signals for its crystalline phase (Fig. S3) and exhibited ca. 60 m^2 g^{-1} of surface area and ca. 0.4 cm^3 g^{-1} of pore volume (Table 1). In the nitrogen physisorption isotherms, the hysteresis loop (Fig. S2) was shifted to higher p_0/p values than for MAP indicating the presence of large mesopores, probably originating from intraparticle voids. Also confirmed by the XRD measurements, the impregnation of palladium did not alter the HAP structure (Fig. S3).

3.2. Crystalline metal species

The MCF support consisted of amorphous silica and did therefore not give any diffraction peaks in the XRD pattern (Fig. S3). Oppositely, Ce-MCF gave after calcination at 500 °C a diffraction pattern corresponding to CeO_2 (28.6˚ (111), 33.1˚ (200), 47.6˚ (220), 56.3˚ (311), 59.2˚ (222), 69.5˚ (400), 76.8˚ (331), 79.1˚ (420), PDF: 00-004-0593) with a calculated particle diameter of 8 nm for the (111) peak using the Scherrer equation [32]. Further impregnation with palladium (calcination at 550 °C) did not provide new, clear diffraction peaks. However, peaks from PdO overlaps with the peak from the (200) crystal plane of CeO_2 (33.1˚) and indeed the shoulder of that peak was broadened for Pd/Ce-MCF which could indicate presence of PdO. The incorporation of niobium and calcium into MCF (Ca-Nb-MCF) resulted in predominant formation of calcium oxide (32.2˚ (111), 37.4˚ (200), 54.0˚ (202), 64.3˚ (311), 67.5˚ (222), PDF: 00-043-1001), calcium hydroxide (34.2˚ (101), 50.9˚ (110), PDF: 00-044-1481) and calcium carbonate (29.4˚ (104), 47.3˚ (102), PDF: 00-005-0586) after calcination at 700 °C. However, after subsequent impregnation with palladium and

calcination at 550 °C only signals from calcium carbonate remained, though the presence of PdO species cannot be excluded if highly dispersed on the surface of the support. Likewise, the original Ca crystalline phases or the PdO phase were not regained when Pd/Ca-Nb-MCF was re-calcined at 700 °C.

The XRD patterns of the reference samples showed a characteristic diffraction pattern of the PdO phase (most intense peak at 33.7˚ (101), PDF: 00-041-1107) for Pd/MAPN while the MAPN was amorphous. On the other hand, the intense diffraction signals originating from the HAP matrix prevented the detection of Pd species by the technique for the Pd/HAP catalyst.

3.3. The state of metal species

XPS was applied to get more insight into the oxidation states of the supported metals in the catalysts. The spectrum of the Pd/Ca-Nb-MCF catalyst (Fig. S4, Table 2) showed symmetric peaks corresponding to palladium oxide (Pd $3d_{3/2}$ at 342.5 eV and Pd $3d_{5/2}$ at 337.3 eV) [33–35]. Moreover, the Nb $3d_{3/2}$ and Nb $3d_{5/2}$ bands at 211.0 and 208.3 eV (Table 2), respectively, indicated the presence of Nb(V). It should be noted that the binding energy observed for Nb had much higher value than typical of niobium(V) oxide, which can be explained by strong metal-support interaction as previously described in literature [36]. This shift has been already documented for niobium loaded onto MCF [20,37]. Moreover, the same phenomenon was observed for Nb-MCF materials doped additionally with calcium [21,38]. The strong metal-support interactions could originate from incorporation of niobium into the structure during the impregnation resulting in the formation of Nb(V)–O– Si bonding [20,36,39]. The region

of Ca 2p (Fig. S4) indicated the presence of 2p doublet with the Ca $2p_{3/2}$ at 347.9 eV typical for the presence of calcium in the form of oxide, carbonate or hydroxide species [40–42]. Notably, all of these species were identified by XRD before incorporation of Pd on the Ca-Nb-MCF support. However, after palladium loading only carbonate species were determined in the XRD pattern, suggesting that the XPS signal was correlated with calcium carbonate species.

The XP spectrum of Pd/Ce-MCF differed from the spectrum of the Pd/Ca-Nb-MCF material (Fig. S4) as two doublets were observed in the Pd 3d region with Pd $3d_{5/2}$ at 335.7 and 337.6 eV and Pd $3d_{3/2}$ at 341.0 and 343.6 eV (Table 2). The signals at 335.7 and 341.0 eV indicated the existence of metallic palladium species on the Ce-MCF support, even though the former value was higher than typically observed for Pd(0). Nevertheless, similar values of binding energy were assigned in literature to metallic palladium species [43,44]. The other two peaks were assigned to PdO, which is in the agreement with the XRD data. The majority (70 %) of palladium was in the form of Pd(0). The XPS data related to cerium were also analyzed (Fig. S4). The coexistence of two different cerium oxidation states resulted in a complex XP spectrum. In literature, it is commonly deconvoluted into five pairs of peaks: three coming from Ce(IV) (v-u, v”-u”, v”’-u”’) and two from Ce(III) (v^0-u^0, v’-u’) [44–46], however, in some studies the Ce(III) doublet v^0-u^0 is not distinguished [47–49]. It was here found difficult to extract the v^0-u^0 doublet in the spectrum of Pd/Ce-MCF, which led to the assumption that Ce(III) species had an insignificant contribution and Ce(IV) species were in the vast majority. As the result the signal in the range from 870 to 925 eV was deconvoluted into three doublets ascribed to Ce(IV), i.e. v-u (882.2-902.2 eV), v’’-u’’ (889.4-910.4 eV) and v’’’-u’’’ (898.3-916.5 eV) and one to Ce(III), i.e. v’-u’ (885.3-906.8 eV).

For the Pd/HAP reference material, the XP spectrum was similar to the Pd/Ce-MCF material showing bands at Pd $3d_{5/2}$ at 335.6 and 336.5 eV (Fig. S4, Table 2) related to metallic palladium (75 %) and palladium oxide (25 %) species. In contrast, the dominant form (67 %) of palladium in Pd/MAPN was identified as palladium oxide giving the band at 336.9 eV whereas Pd(0) was detected at 335.7 eV of Pd $3d_{5/2}$ (Table 2). The major presence of PdO in Pd/MAPN is in agreement with the XRD data obtained for this material.

3.4. Catalyst basicity

The basicity of the materials were evaluated by CO_2-TPD measurements. The corresponding CO_2 desorption profiles of each catalyst are presented in Fig. 1 and the calculated basic sites are compiled in Table 3. Both of the MCF supports modified with Ce or Ca-Nb showed similar basicity (rather week) as demonstrated by the same temperature of CO_2 desorption (i.e. 93 °C). However, for the Ce-MCF material two additional desorption peaks were observed at 284 and 416 °C corresponding to medium and high strength basic sites, respectively, which is in agreement with literature data related to CeO_2 [4]. These two additional peaks seemed to disappear after modification with palladium, however, simultaneously the intensity of the desorption peak around 93 °C increased. A similar increase in intensity was observed after incorporation of palladium in the Ca-Nb-MCF support.

The basicity of the reference materials differed from those based on MCF. Unmodified MAP exhibited very low basicity (Fig. 1), while the oxynitride material MAPN (as expected) gave a strong basicity desorption peak that could be deconvoluted into three

peaks at 137, 215 and 313 °C related to various basic sites, respectively. The latter peaks at 215 and 313 °C moved to lower temperatures (185 and 280 °C) after incorporation of palladium, which likely indicated a decrease in the basic strength of these sites. The second reference material HAP showed similar strength of the basic sites as the MCF-based supports, however, the number of basic sites were higher. Nevertheless, for Pd/HAP, in contrast to the MCF catalysts, the desorption peak was shifted towards higher temperature (121 °C) after palladium impregnation suggesting that the basic sites were stronger after palladium incorporation.

3.5. Catalyst performance

The catalytic performance of the modified palladium catalysts was examined for gas phase conversion of acetone to MIBK at four different temperatures (150, 200, 250 and 300 °C) and the obtained results are presented in Fig. 2. For the Pd/Ca-Nb-MCF catalyst, the acetone conversion gradually increased with increasing temperature (as expected) reaching the highest conversion of 10.9 % at 300 °C with high selectivity of 94-100 % to MIBK at all temperatures. Formation of diisobutyl ketone (DIBK) by consecutive condensation of acetone with MIBK was a minor byproduct. In comparison, the Pd/Ce-MCF catalyst exhibited much higher activity than Pd/Ca-Nb-MCF providing an acetone conversion of 31.6 % at 300 °C while maintaining a high MIBK selectivity of 86 %. DIBK formed also here as the major byproduct (13 % at 300 °C).

The Pd/HAP reference catalyst was confirmed to be an efficient catalyst for acetone condensation as also reported in literature [9,10], giving high acetone conversion at 250

°C (30.3 %) with a high selectivity to MIBK (87 %). Like for the Pd/Ce-MCF catalyst, DIBK formation was also here observed (selectivity 13 %). However, in contrast to the latter catalyst did the activity of the Pd/HAP catalyst only increase moderately at higher temperature of 300 °C. For both of the catalysts did the selectivity to MIBK generally decrease with acetone conversion as shown in Fig. S5.

For the Pd/MAPN catalyst was the reaction selectivity markedly different as the main product (>90 % selectivity) was diisopropyl ether (DIPE) at lower temperatures and isopropyl alcohol (IPA) at higher temperature. The desired product MIBK only started forming at 300 °C and with a low selectivity of 26 %. Ether formation is known to take place on acidic sites [50,51] while isopropyl alcohol forms on metallic sites [52], suggesting that more acidic than basic sites were present in the oxynitride catalyst where P-OH groups are supposed to be converted to P-NH_2 [26]. To confirm this hypothesis, 2,5-hexanedione cyclisation and dehydration was performed as a test reaction, where 2,5-dimethylfuran (DMF) form over acidic sites and 3-methyl-2-cyclopentenone (MCP) over basic sites [53]. In the test reaction, 12 % of the 2,5-hexanedione was converted into a product with high selectivity to DMF (66 %) (Table S1) implying major contribution of acidic sites in the Pd/MAPN catalyst. In contrary, the base-catalyzed product, MCP, was mainly formed (99 %) over other catalysts which were also highly selective to MIBK (Pd/Ca-Nb-MCF, Pd/Ce-MCF and Pd/HAP).

Notably, the best catalyst supports (HAP, Ca-Nb-MCF and Ce-MCF) provided without incorporated palladium mesityl oxide (MO) as the main product and only low selectivity towards MIBK formation (around 10 %) (Fig. S6). Thus, it was obvious that the addition of palladium nanoparticles was crucial for MIBK formation with the catalysts. Moreover, the best catalytic performance was observed for the samples were

the dominant form of palladium was Pd(0) according to the XPS data, i.e. Pd/Ce-MCF and Pd/HAP. However, it was also apparent that there was no direct correlation between catalyst selectivity to MIBK and basicity of the catalyst estimated by the CO_2-TPD method (Table 3). Such correlation was found, for instance, in case of CeO_2 modified with Ni [4]. Hence, possibly not all basic sites measured by the CO_2 adsorption took part in the transformation of acetone. Nevertheless, the higher number of basic sites in Pd/Ca-Nb-MCF than Pd/Ce-MCF estimated by the CO_2-TPD technique was reflected by the increase in activity in 2,5-hexanedione cyclization (14 vs 9 % of conversion, Table S1). Interestingly, the conversion of acetone with Ca-Nb-MCF support was similar to the conversion with Ce-MCF and HAP supports, while the activity of Pd/Ce-MCF and Pd/HAP after modification with palladium was notably better than Pd/Ca-Nb-MCF especially at high temperature. However, for MIBK formation both basic and hydrogenation active sites are necessary. According to the XPS data the superior catalysts exhibited partially reduced palladium which facilitated the high yield of MIBK.

3.6. Catalyst stability

Pd/HAP and Pd/Ce-MCF were found to be the most active catalysts of the studied materials at higher temperature, and their durability were therefore tested in longer termed continuous reactions of 24 h. The results are presented in Fig. 3. The literature does not provide data of long term stability of HAP catalysts in the acetone condensation reaction, however, it was shown that the conversion of acetone continuously decreased during 3 h of reaction time [9]. In line with this, the activity of

the Pd/HAP catalyst was also here found to drastically decrease within the first 3 h of reaction and the catalyst had after 24 h of reaction lost ca. 70 % of its initial activity (decrease in conversion from ca. 27 to 8 %). Nevertheless, the selectivity remained high throughout the reaction even with a noticeable enhancement of the selectivity to MIBK. The acetone conversion with the Pd/Ce-MCF catalyst was initially somewhat lower than the conversion with Pd/HAP (11 % vs. 27 %), however, the catalyst remained highly stable during the 24 h of continuous reaction with essentially unchanged performance. The difference in the stability of the active samples studied in this work may be related to the more open structure of the MCF support allowing a possibly better separation of active sites. Furthermore, the mesoporous structure could contribute to the dispersion of active sites which bases on TEM images seemed to be better in as-synthesized Pd/Ce-MCF than in Pd/HAP (Fig. S7).

Elemental analysis of the catalysts after the stability test showed that more coke was deposited on Pd/Ce-MCF (3.4 % carbon) than on Pd/HAP (0.3 % carbon). Moreover, the textural properties of the spent catalysts differed from the as-synthesized samples (Table S2) as the BET was decreased by 25 % for Pd/Ce-MCF and by 17 % for Pd/HAP. A similar trend was also observed for the pore volumes, which were reduced by 30 and 22 % for Pd/Ce-MCF and Pd/HAP, respectively, due to the deposited carbon species. Despite the Pd/Ce-MCF catalyst contained more residues formed during the reaction likely partially blocking the pores, the catalyst still performed better than Pd/HAP due to the high surface area and larger pores of the MCF structure allowing an efficient flux of reagents. Accordingly, the Pd/Ce-MCF catalyst was a durable and attractive alternative compared to Pd/HAP, which deactivated rapidly over time.

4. Conclusion

New palladium containing catalysts based on Ce-MCF and Ca-Nb-MCF supports were prepared and characterized. The incorporation of metal dopants in the support decreased the surface area as well as pore diameter of the supports, however the mesoporous structures of the foams were maintained. Additional incorporation of palladium in small amount influenced the structure parameters and different forms of palladium were obtained in the final materials. Hence, the majority of metallic palladium species (similar as for Pd/HAP) were detected in Pd/Ce-MCF whereas PdO species were determined in the case of Pd/Ca-Nb-MCF (similar as for Pd/MAPN). The state of palladium species as well as basicity of the materials strongly influenced the catalytic performance of the resulting catalysts in the gas-phase conversion of acetone to MIBK. A reference Pd/HAP catalyst showed the best initial catalytic performance, but its activity rapidly decreased over time during reaction. In contrary, the catalyst based on the Ce-MCF support maintained its initial activity and selectivity during the reaction for at least 24 h proving Pd/Ce-MCF to be the most attractive catalyst for the abovementioned process. More detailed understanding of the Pd/Ce-MCF stability will be objective for future research.

Acknowledgements

The work was supported by grant no. POWR.03.02.00-00-I026/16 co-financed by the European Union through the European Social Fund under the Operational Program Knowledge Education Development.

Appendix A. Supplementary data

Characterization data (nitrogen adsorption/desorption isotherms and textural data, XRD, XPS, TEM, SEM) and catalytic data of supports and Pd-catalysts.

Supplementary data to this article is available online at xxx.

References

[1] R. Banavali, M.J. Deetz, A.K. Schultz, in: J. Tulla-Puche, F. Albericio (Eds.), The Power of Functional Resins in Organic Synthesis, WILEY-VCH, Weinheim, 2008, p. 322. https://doi.org/10.1002/9783527626175.

[2] V. Chikán, Á. Molnár, K. Balázsik, J. Catal. 184 (1999) 134–143. https://doi.org/10.1006/jcat.1999.2437.

[3] B.Y. Coh, J.M. Hur, H.I. Lee, Stud. Surf. Sci. Catal. 121 (1999) 453–456. https://doi.org/10.1016/s0167-2991(99)80117-7.

[4] P.V.R. Rao, V.P. Kumar, G.S. Rao, K.V.R. Chary, Catal. Sci. Technol. 2 (2012) 1665–1673. https://doi.org/10.1039/c2cy20021j.

[5] Y.Z. Chen, B.J. Liaw, H.R. Tan, K.L. Shen, Appl. Catal. A Gen. 205 (2001) 61–69. https://doi.org/10.1016/S0926-860X(00)00545-7.

[6] D. Bomboş, G. Bozga, M. Bomboş, A. Ştefan, I. Stanciu, Chem. Pap. 54 (2000) 171–176.

[7] R. Pulikkal Thumbayil, J. Mielby, S. Kegnæs, Top. Catal. 62 (2019) 678–688. https://doi.org/10.1007/s11244-019-01153-6.

[8] A.A. Nikolopoulos, B.W.L. Jang, J.J. Spivey, Appl. Catal. A Gen. 296 (2005) 128–136. https://doi.org/10.1016/j.apcata.2005.08.022.

[9] N. Cheikhi, M. Kacimi, M. Rouimi, M. Ziyad, L.F. Liotta, G. Pantaleo, G. Deganello, J. Catal. 232 (2005) 257–267. https://doi.org/10.1016/j.jcat.2005.03.016.

[10] C.R. Ho, S. Zheng, S. Shylesh, A.T. Bell, J. Catal. 365 (2018) 174–183. https://doi.org/10.1016/j.jcat.2018.07.005.

[11] G. Waters, O. Richter, B. Kraushaar-Czarnetzki, Ind. Eng. Chem. Res. 45 (2006) 5701–5707. https://doi.org/10.1021/ie060184b.

[12] L.M. Gandía, R. Malm, R. Marchand, R. Conanec, Y. Laurent, M. Montes, Appl. Catal. A, Gen. 114 (1994) L1–L7. https://doi.org/10.1016/0926-860X(94)85105-0.

[13] S.M. Yang, Y.M. Wu, Appl. Catal. A Gen. 192 (2000) 211–220. https://doi.org/10.1016/S0926-860X(99)00408-1.

[14] T. Richardson, James, Principles of Catalyst Development, Springer US, 1989. https://doi.org/10.1007/978-1-4899-3725-4.

[15] T. Tsoncheva, L. Ivanova, J. Rosenholm, M. Linden, Appl. Catal. B Environ. 89 (2009) 365–374. https://doi.org/10.1016/j.apcatb.2008.12.015.

[16] L. Hermida, J. Agustian, A.Z. Abdullah, A.R. Mohamed, Open Chem. 17 (2019) 1000–1016. https://doi.org/10.1515/chem-2019-0107.

[17] A. Held, E. Janiszewska, J. Czerepińska, J. Kowalska-Kuś, RSC Adv. 10 (2020) 10144–10154. https://doi.org/10.1039/d0ra00349b.

[18] M. Trejda, K. Stawicka, M. Ziolek, Catal. Today. 192 (2012) 130–135. https://doi.org/10.1016/j.cattod.2012.02.042.

[19] P. Schmidt-Winkel, W.W. Lukens, Jr., D. Zhao, P. Yang, B.F. Chmelka, G.D. Stucky, J. Am. Chem. Soc. 121 (1999) 254–255.

https://doi.org/10.1021/ja983218i.

[20] K. Stawicka, P. Decyk, A. Wojtaszek-Gurdak, M. Ziolek, Catal. Today. 325 (2019) 2–10. https://doi.org/10.1016/j.cattod.2018.05.025.

[21] D. Kryszak, M. Trejda, N. Benedyczak, M. Ziolek, Catal. Today. 325 (2019) 11–17. https://doi.org/10.1016/j.cattod.2018.05.054.

[22] E.G. Rodrigues, T.C. Keller, S. Mitchell, J. Pérez-Ramírez, Green Chem. 16 (2014) 4870–4874. https://doi.org/10.1039/c4gc01432d.

[23] A. Toso, S. Colussi, S. Padigapaty, C. de Leitenburg, A. Trovarelli, Appl. Catal. B Environ. 230 (2018) 237–245. https://doi.org/10.1016/j.apcatb.2018.02.049.

[24] M. Boutros, M.E. Gálvez, T. Onfroy, P. Da Costa, Microporous Mesoporous Mater. 183 (2014) 1–8. https://doi.org/10.1016/j.micromeso.2013.08.031.

[25] M. Thommes, K. Kaneko, A. V. Neimark, J.P. Olivier, F. Rodriguez-Reinoso, J. Rouquerol, K.S.W. Sing, Pure Appl. Chem. 87 (2015) 1051–1069. https://doi.org/10.1515/pac-2014-1117.

[26] M.J. Climent, A. Corma, V. Fornés, R. Guil-Lopez, S. Iborra, Adv. Synth. Catal. 344 (2002) 1090–1096. https://doi.org/10.1002/1615-4169(200212)344:10<1090::AID-ADSC1090>3.0.CO;2-X.

[27] J.J. Benítez, A. Díaz, Y. Laurent, J.A. Odriozola, Catal. Letters. 54 (1998) 159–164. https://doi.org/10.1023/A:1019052627424.

[28] J.A. Odriozola, J.J. Benítez, P. Grange, Y. Laurent, R. Marchand, J. Chem. Soc., Faraday Trans. 91 (2004) 4477–4479. https://doi.org/10.1039/ft9959104477.

[29] M.J. Climent, A. Corma, V. Fornés, A. Frau, R. Guil-López, S. Iborra, J. Primo, J. Catal. 163 (2002) 392–398. https://doi.org/10.1006/jcat.1996.0340.

[30] M.A. Centeno, M. Debois, P. Grange, J. Catal. 192 (2000) 296–306.

https://doi.org/10.1006/jcat.2000.2848.

[31] J. Wang, Q. Liu, J. Mater. Res. 22 (2007) 3330–3337. https://doi.org/10.1557/jmr.2007.0436.

[32] A.L. Patterson, Phys. Rev. 56 (1939) 978–982. https://doi.org/10.1103/PhysRev.56.978.

[33] S. Niu, W. Guo, T.W. Lin, W. Yu, Y. Wu, X. Ji, L. Shao, RSC Adv. 7 (2017) 25885–25890. https://doi.org/10.1039/c7ra03665e.

[34] C. Wang, F. Yang, W. Yang, L. Ren, Y. Zhang, X. Jia, L. Zhang, Y. Li, RSC Adv. 5 (2015) 27526–27532. https://doi.org/10.1039/c4ra16792a.

[35] M. Muniz-Miranda, A. Zoppi, F. Muniz-Miranda, N. Calisi, Coatings. 10 (2020) 207. https://doi.org/10.3390/coatings10030207.

[36] M. Ziolek, Catal. Today. 78 (2003) 47–64. https://doi.org/10.1016/S0920-5861(02)00340-1.

[37] L. Wolski, I. Sobczak, M. Ziolek, Microporous Mesoporous Mater. 243 (2017) 339–350. https://doi.org/10.1016/j.micromeso.2017.02.038.

[38] K. Grzelak, M. Ziolek, M. Trejda, Catal. Commun. 142 (2020). https://doi.org/10.1016/j.catcom.2020.106045.

[39] M. Ziolek, I. Sobczak, Catal. Today. 285 (2017) 211–225. https://doi.org/10.1016/j.cattod.2016.12.013.

[40] B. Demri, D. Muster, J. Mater. Process. Tech. 55 (1995) 311–314. https://doi.org/10.1016/0924-0136(95)02023-3.

[41] D.K. Dumbre, V.R. Choudhary, N.S. Patil, B.S. Uphade, S.K. Bhargava, J. Colloid Interface Sci. 415 (2014) 111–116. https://doi.org/10.1016/j.jcis.2013.10.016.

[42] M.C.G. Albuquerque, I. Jiménez-Urbistondo, J. Santamaría-González, J.M. Mérida-Robles, R. Moreno-Tost, E. Rodríguez-Castellón, A. Jiménez-López, D.C.S. Azevedo, C.L. Cavalcante Jr., P. Maireles-Torres, Appl. Catal. A Gen. 334 (2008) 35–43. https://doi.org/10.1016/j.apcata.2007.09.028.

[43] X. Wang, J. Chen, J. Zeng, Q. Wang, Z. Li, R. Qin, C. Wu, Z. Xie, L. Zheng, Nanoscale. 9 (2017) 6643–6648. https://doi.org/10.1039/c6nr09707c.

[44] A.I. Boronin, E.M. Slavinskaya, I.G. Danilova, R. V. Gulyaev, Y.I. Amosov, P.A. Kuznetsov, I.A. Polukhina, S. V. Koscheev, V.I. Zaikovskii, A.S. Noskov, Catal. Today. 144 (2009) 201–211. https://doi.org/10.1016/j.cattod.2009.01.035.

[45] X.S. Huang, H. Sun, L.C. Wang, Y.M. Liu, K.N. Fan, Y. Cao, Appl. Catal. B Environ. 90 (2009) 224–232. https://doi.org/10.1016/j.apcatb.2009.03.015.

[46] J.M. Sánchez-Amaya, G. Blanco, F.J. Garcia-Garcia, M. Bethencourt, F.J. Botana, Surf. Coatings Technol. 213 (2012) 105–116. https://doi.org/10.1016/j.surfcoat.2012.10.027.

[47] L. Escamilla-Perea, R. Nava, B. Pawelec, M.G. Rosmaninho, C.L. Peza-Ledesma, J.L.G. Fierro, Appl. Catal. A Gen. 381 (2010) 42–53. https://doi.org/10.1016/j.apcata.2010.03.038.

[48] L.F. Liotta, G. Pantaleo, F. Puleo, A.M. Venezia, Catal. Today. 187 (2012) 10–19. https://doi.org/10.1016/j.cattod.2012.01.001.

[49] K. Kuntaiah, P. Sudarsanam, B.M. Reddy, A. Vinu, RSC Adv. 3 (2013) 7953–7962. https://doi.org/10.1039/c3ra23491f.

[50] R.J. Taylor, P.S.E. Dai, J.F. Knifton, Catal. Letters. 68 (2000) 1–5. https://doi.org/10.1023/A:1019023201520.

[51] F. Zaccheria, N. Scotti, N. Ravasio, Catalysts. 9 (2019).

https://doi.org/10.3390/catal9020172.

[52] K.I. Shimizu, Catal. Sci. Technol. 5 (2015) 1412–1427.

https://doi.org/10.1039/c4cy01170h.

[53] R.M. Dessau, Zeolites. 10 (1990) 205–206.

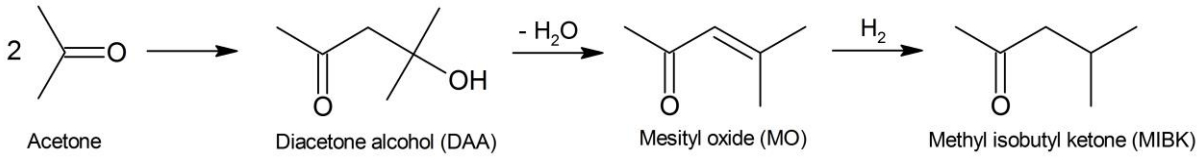

Scheme 1. Synthesis of methyl isobutyl ketone from acetone.

Table 1. Textural parameters of supports and catalysts.

Catalyst	BET surface area ($m^2\ g^{-1}$)	Pore diameter (nm)		Pore volume ($cm^3\ g^{-1}$)
		adsorption	desorption	
MCF [a]	716	24.3	15.7	2.17
Ca-Nb-MCF [a]	276	22.9	11.1	1.03
Pd/Ca-Nb-MCF [a]	206	21.9	12.8	0.87
Ce-MCF [a]	487	22.4	15.6	1.58
Pd/Ce-MCF [a]	493	21.7	12.3	1.31
HAP [b]	61	30.6	-	0.38
Pd/HAP [b]	58	31.2	-	0.37
MAP [c]	274	11.8	-	0.46
MAPN [c]	125	11.8	-	0.26
Pd/MAPN [c]	119	10.1	-	0.23

[a] Pore volume and cell diameter determined from adsorption branches of N_2 isotherms. Window diameter determined from desorption branches of N_2 isotherms by BdB-Fass method. [b] Pore volume and diameter determined from adsorption branches of N_2 isotherms by BJH method with Kruk-Jaroniec-Sayaroi correction. [c] Pore volume and diameter determined from adsorption branches of N_2 isotherms by DFT method.

Table 2. XPS bands positions of the Pd-catalysts in the Pd 3d region.

Catalyst	Pd $3d_{5/2}$ (eV)		Pd $3d_{3/2}$ (eV)	
Pd/Ca-Nb-MCF		337.3		342.5
Pd/Ce-MCF	335.7	337.6	341.0	343.6
Pd/HAP	335.6	336.5	341.0	342.0
Pd/MAPN	335.7	336.9	341.2	342.1

Table 3. CO_2-TPD data combined with activity of Pd-catalysts for MIBK formation.

Catalyst	Yield of MIBK (%) [a]	Desorbed CO_2 (mmol $g_{cat}^{-1} \cdot 10^{-3}$)
Pd/Ca-Nb-MCF	10.2	3.36
Pd/Ce-MCF	27.2	2.02
Pd/HAP	29.9	3.79
Pd/MAPN	7.5	2.90

[a] Reaction conditions: Acetone (0.05 cm^3 min^{-1}), hydrogen (50 cm^3 min^{-1}), ambient pressure, 300 °C.

Figure captions

Fig. 1. CO_2-TPD profiles of supports and Pd-catalysts.

Fig. 2. Catalytic performance of Pd-catalysts in the conversion of acetone to MIBK (IPA: isopropyl alcohol, DIBK: diisobutyl ketone, DIPE: diisopropyl ether). Reaction conditions: acetone (0.05 cm^3 min^{-1}), hydrogen (50 cm^3 min^{-1}), ambient pressure.

Fig. 3. Stability tests for Pd/Ce-MCF and Pd/HAP catalysts in the conversion of acetone to MIBK (IPA: isopropyl alcohol, DIBK: diisobutyl ketone). Reaction conditions: acetone (0.05 cm^3 min^{-1}), hydrogen (50 cm^3 min^{-1}), ambient pressure, 250 °C.

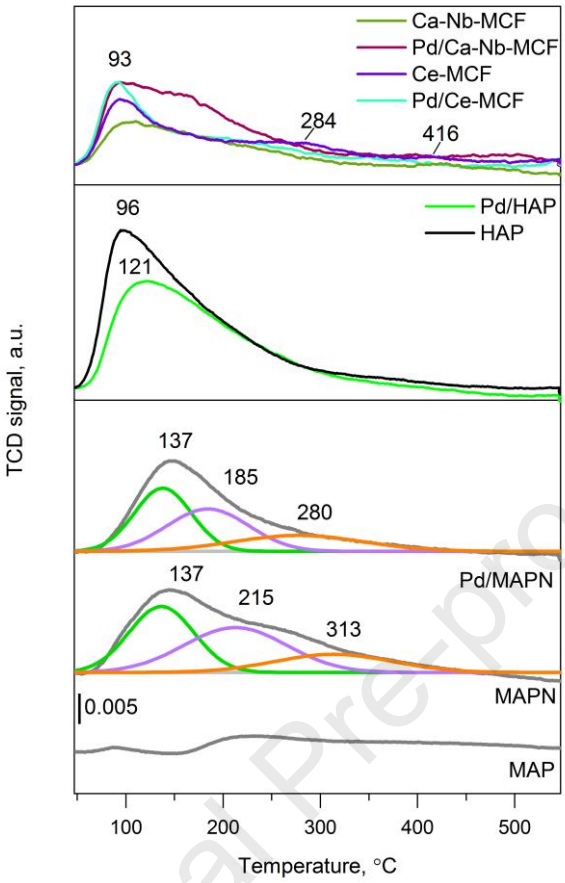

Fig. 1.

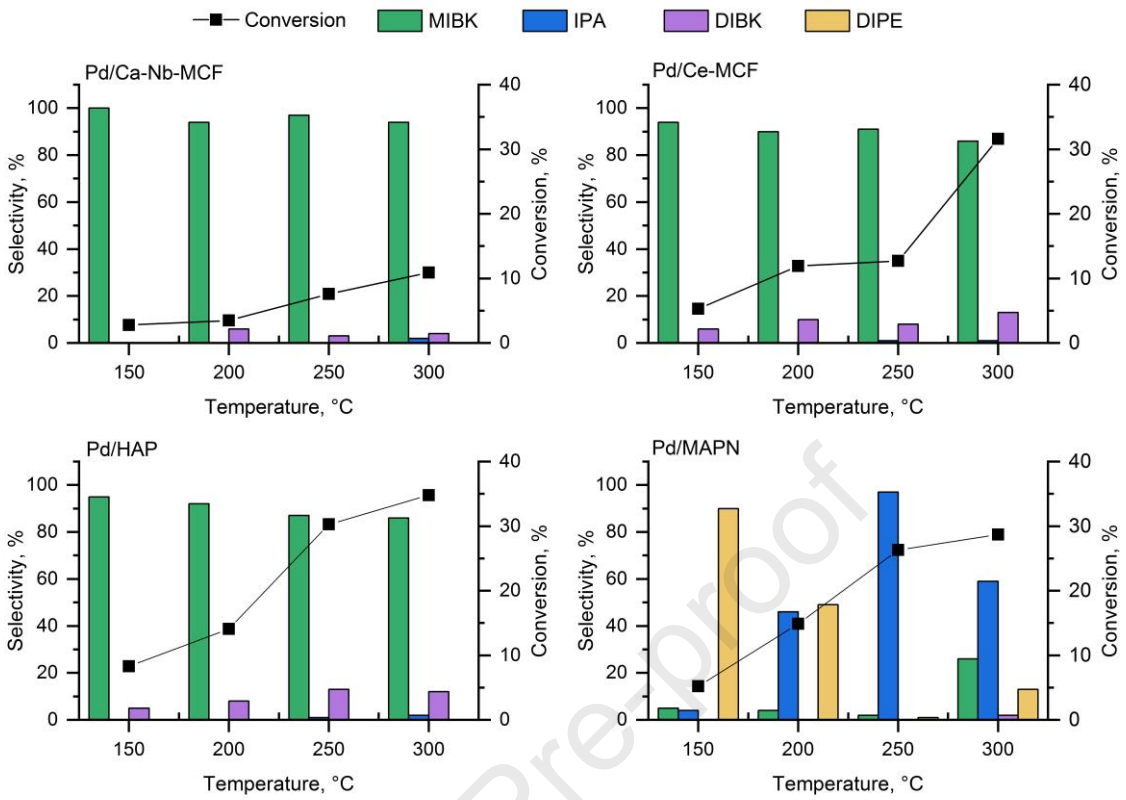

Fig. 2.

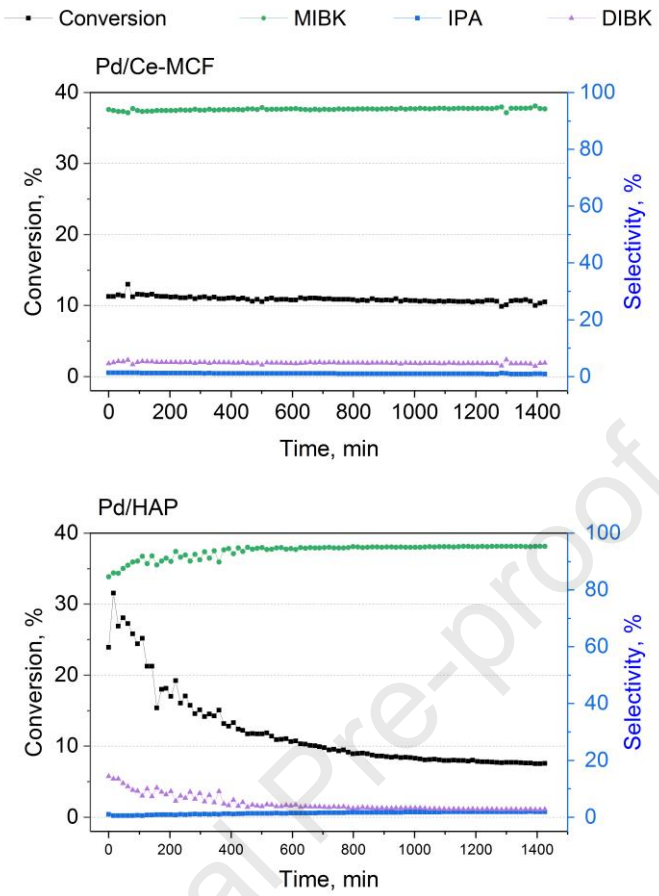

Fig. 3.

Highlights

- Palladium was impregnated on cerium and calcium-niobium doped MCF support
- The oxidation state of palladium was influenced by the MCF support composition
- Both the state of palladium and sample basicity had impact on catalytic performance
- Pd/Ce-MCF demonstrated superior catalyst stability over prolonged reaction time

Declaration of Interest Statement

The authors declare that they have no known competing financial interests or personal relationships that could have appeared to influence the work reported in this paper.